Broad cross-species infection of cultured cells by the bat HKU2-related swine acute diarrhea syndrome coronavirus (SADS-CoV) and identification of its replication in murine dendritic cells *in vivo* highlight its potential for diverse interspecies transmission

Yong-Le Yang,[a]* Pan Qin,[a]* Bin Wang,[a] Yan Liu,[a] Guo-Han Xu,[a] Lei Peng,[a] Jiyong Zhou,[a] Shu Jeffrey Zhu,[a]# Yao-Wei Huang[a]#

[a]Key Laboratory of Animal Virology of Ministry of Agriculture and Institute of Preventive Veterinary Medicine, Department of Veterinary Medicine, Zhejiang University, Hangzhou 310058, Zhejiang, China.

*These authors contributed equally to this work.

#Address correspondence to

Dr. Yao-Wei Huang, Zhejiang University, yhuang@zju.edu.cn

Dr. Shu Jeffrey Zhu, Zhejiang Univeristy, shuzhu@zju.edu.cn

Running title: Broad species tropism and a mouse model of SADS-CoV

Word counts: manuscript text (5,908 words); abstract (250 words); importance (139 words).

Figure number: 6; **Table number**: 1

ABSTRACT

Outbreaks of severe diarrhea in neonatal piglets in Guangdong, China in 2017 resulted in isolation and discovery of a novel swine enteric alphacoronavirus (SeACoV) derived from the species *Rhinolophus bat coronavirus HKU2* (Vet Microbiol, 2017, 211:15-21). SeACoV was later referred to as swine acute diarrhea syndrome (SADS) CoV by another group (Nature, 2018, 556:255-258). The present study was set up to investigate potential species barriers of SADS-CoV *in vitro* and *in vivo*. We first demonstrated that SADS-CoV possesses a broad species tropism and is able to infect cell lines from diverse species including bats, mice, rats, gerbils, hamsters, pigs, chickens, nonhuman primates and humans. Trypsin contributes to, but is not essential for SADS-CoV propagation *in vitro*. Furthermore, C57BL/6J mice were inoculated with the virus via oral or intraperitoneal routes. Although the mice exhibited only subclinical infection, they supported viral replication and prolonged infection in the spleen. SADS-CoV nonstructural proteins and double-stranded RNA were detected in splenocytes of the marginal zone on the edge of lymphatic follicles, indicating active replication of SADS-CoV in the mouse model. We identified that splenic dendritic cells (DCs) are the major targets of virus infection by immunofluorescence and flow cytometry approaches. Finally, we demonstrated that SADS-CoV does not utilize known CoV receptors for cellular entry. The ability of SADS-CoV to replicate in various cells lines from a broad range of species and the unexpected tropism for murine DCs provide important insights into the biology of this bat-origin CoV, highlighting its possible ability to cross interspecies barriers.

43 **IMPORTANCE**

44 Infections with bat-origin CoVs (SARS-CoV and MERS-CoV) have caused severe illness
45 in humans after "host jump" events. Recently, a novel bat-HKU2-like CoV named swine acute
46 diarrhea syndrome CoV (SADS-CoV) has emerged in southern China, causing a lethal diarrhea
47 in newborn piglets. It is important to assess the species barriers of SADS-CoV infection since the
48 animal hosts (other than pigs and bats) and zoonotic potential are still unknown. An *in vitro*
49 susceptibility study revealed a broad species tropism of SADS-CoV, including various rodent
50 and human cell lines. We established a mouse model of SADS-CoV infection, identifying its
51 active replication in splenic dendritic cells, which suggests that SADS-CoV has the potential to
52 infect rodents. These findings highlight the potential cross-species transmissibility of SADS-CoV,
53 though further surveillance in other animal populations is needed to fully understand the ecology
54 of this bat-HKU2-origin CoV.

55

56 **Keywords:** Interspecies transmission; Coronavirus; SADS-CoV; Mouse infection model

57

58

INTRODUCTION

The spread of zoonotic pathogens remains among the leading threats to global public health. Coronaviruses (CoVs) can infect a wide variety of animals and humans, resulting in several diseases with respiratory, enteric, and neurological pathologies of varying severity (1-4). Because of the various routes of infection and extensive phagocytosis in tissues, close contact between humans and animals provides potential scenarios for adaptive mutation and interspecies transmission (5).

The source of the severe acute respiratory syndrome (SARS)-CoV was traced to civets in animal markets and ultimately to bats, leading to more than 8,000 human infections and 774 deaths after its emergence in 2002 (5-7). The emergence of Middle East respiratory syndrome (MERS)-CoV in 2012 (2) resulted in more than 1,000 clinical cases with a mortality rate of 35%, making it the second marked threatening CoV of the 21st century (8, 9). Although camels can be infected with MERS-CoV, bats are also thought to be the original host of MERS-CoV (5). Both SARS-CoV and MERS-CoV originated in bats, illustrating the damage caused by CoVs during interspecies transmission events, and highlighting the need for increased global vigilance of CoV-associated disease (1, 5, 10).

In February 2017, outbreaks of severe diarrhea of suckling piglets occurred in swine herds in Guangdong Province, China (11). Clinical signs consisted of acute vomiting and watery diarrhea, but porcine viruses commonly associated with diarrhea including porcine epidemic diarrhea virus (PEDV), transmissible gastroenteritis virus (TGEV) and porcine deltacoronavirus (PDCoV) were not detected in any of the clinical samples (11). The new enteric pathogen of

commercial pigs that was isolated was finally identified as a new porcine CoV belonging to the species *Rhinolophus bat coronavirus HKU2* (11-13). Our research group tentatively designated this newly emerged virus as swine enteric alphacoronavirus (SeACoV) (11), and it was later named swine acute diarrhea syndrome (SADS)-CoV by Zhou *et al.* (14). It is also known by other names, such as porcine enteric alphacoronavirus (PEAV) (13). For purposes of unity, SADS-CoV is the name used to refer to this new virus in the current study. The expanded host range of bat-origin HKU2 to pigs indicates that bats play an important role in the ecology and evolution of SADS-CoV, though the mechanism of bat-to-swine transmission remains unclear. In view of the damage caused by SARS and MERS for both animal and public health, careful attention must be paid to the prevalence of CoV-associated disease among humans and domestic animals (15).

Therefore, there is an urgent need for more information on the details of SADS-CoV infection. It is critically important to assess potential species barriers of SADS-CoV transmission since the animal hosts (other than pigs and bats) and zoonotic potential are still unknown. In the present study, we demonstrated that SADS-CoV possesses a very broad species tropism *in vitro* and is able to infect cell lines from diverse species including rodents and humans. Furthermore, *in vivo* evidence from experimental infection of mice with SADS-CoV identified splenic dendritic cells (DCs) as the major site of SADS-CoV replication in mice. Finally, we demonstrated that SADS-CoV does not utilize known CoV protein receptors for cellular entry. These results present the possibility that rodents are among the susceptible hosts of SADS-CoV, highlighting the potential cross-species transmissibility of SADS-CoV.

MATERIALS AND METHODS

Virus stocks and viral antibodies. The SADS-CoV isolate CH/GD-01/2017 at passage 10 was used in all experiments and cultured in Vero cells (16). The virus was passaged serially using the culture supernatant to infect fresh Vero cells at a multiplicity of infection (MOI) of 0.1, and viral titers were determined in Vero cells by endpoint dilution as the 50% tissue culture infective dose 50% ($TCID_{50}$). Rabbit polyclonal antibodies (pAb) against the membrane (M), nucleocapsid (N) and the nonstructural protein 3 (Nsp3) acidic domain (AC) of SADS-CoV were generated in-house, and validated in SADS-CoV-infected Vero cells (16). A mouse anti-SADS-CoV-N pAb was also produced to allow double staining when mixed with the rabbit pAb. A monoclonal antibody (MAb) against dsRNA (anti-dsRNA mAb J2, Cat# J2-1702, SCICONS, Hungary) was used to specifically detect viral replication of SADS-CoV.

Cell lines and cell culture. Twenty-four cell lines derived from tissues of different species were used (Table 1), including human (Huh-7, HepG2/C3A, 293T, A549 and HeLa), monkey (Marc-145, Cos-7, BSC-40, Vero), swine [ST, PK15, LLC-PK1, IPEC-J2 (17)], bat [BFK (18), Tb-1], canine (MDCK), mouse (NIH/3T3, RAW 264.7), hamster (BHK-21, CHO), rat (BRL-3A, NRK-52E), chicken (DF-1) cell lines and a primary kidney cell line from Mongolian gerbils (prepared in-house). The BFK cell line was a generous gift from Dr. Changchun Tu at the Institute of Military Veterinary Medicine, Changchun, China. Each cell line was cultured in Dulbecco's modified Eagle's medium (DMEM, Hyclone) supplemented with 10% (v/v) fetal bovine serum (FBS, Biological Industries), 100 U/ml penicillin and 100 U/ml streptomycin at

122 37 °C, 5% CO_2, and water-saturated humidity conditions.

123 To determine viral susceptibility, each cell line was cultured at 70% confluence in 12-well
124 plates with maintenance medium (MM) containing DMEM, 0.3% tryptose phosphate broth
125 (TPB), and 1% penicillin/streptomycin, or MM with addition of 5 μg/ml trypsin (MMT) (Sigma,
126 Cat#T7186-50TAB, St Louis, MO, USA). After washing with phosphate buffered saline (PBS),
127 cells were inoculated with SADS-CoV diluted in MM or MMT at an MOI of 0.01 for 2 h.
128 Non-attached viruses were removed by washing the cells three times with DMEM, and cell
129 monolayers were subsequently incubated in MM or MMT at 37 °C for 5 days. To determine the
130 effect of trypsin on viral entry, cell monolayers were infected by SADS-CoV in three conditions:
131 1) no trypsin treatment, infected with SADS-CoV diluted in MM, subsequently incubated in MM;
132 2) pre-trypsin treatment, inoculated with SADS-CoV diluted in MMT, subsequently incubated in
133 MM; and 3) double-trypsin treatment, inoculated with SADS-CoV in MMT, subsequently
134 incubated in MMT. Supernatants from cells were collected at 12, 24, 36, 48, 72, and 120 hours
135 post-infection (hpi) for one-step quantitative RT-PCR analysis. Cell cultures were examined for
136 cytopathic effects (CPE) and immunofluorescence assay at 48-72 hpi.

137 **Immunofluorescence assay (IFA) for cell line susceptibility.** Different cells infected with
138 SADS-CoV in 12-well plates were washed twice with PBS and fixed in 4% paraformaldehyde in
139 PBS and then permeabilized with 0.1% Triton X-100 in PBS. Cells were then incubated with the
140 rabbit anti-SADS-CoV-M pAb at 1:5000 dilution for 1 h at 37 °C, washed with PBS and stained
141 with the Alexa Fluor 488-conjugated goat anti-rabbit secondary antibody (Thermo Fisher
142 Scientific, USA) at 1:1000 dilution. After incubation for 1 h at 37 °C, the cells were washed with

143 PBS, stained with 4′,6-diamidino-2-phenylindole (DAPI) at 1:1000 dilution and visualized on a
144 fluorescence microscope.

145 **One-step quantitative RT-PCR analysis targeting the N gene.** The full-length SADS-CoV
146 N gene was inserted into an appropriately digested pET-28a vector using two unique restriction
147 sites, *Nde*I and *Xho*I, and then linearized with *Xho*I. The N gene was *in vitro* transcribed using
148 the T7 High Efficiency Transcription Kit (TransGen Biotech Co., LTD, Beijing China). Standard
149 curves were generated using dilutions of known quantity of N gene RNA to allow absolute
150 quantitation of SADS-CoV RNA copy numbers in samples.

151 Total RNA was extracted from culture supernatants or tissue homogenates using Trizol
152 (ThermoFisher Scientific, USA) following the manufacturer's instructions. SADS-CoV RNA
153 titer was determined by one-step qRT-PCR (TOYOBO Co., LTD) targeting the N gene with the
154 primers: 5'-CTAAAACTAGCCCCACAGGTC-3' and 5'-TGATTGCGAGAACGAGACTG-3',
155 and the probe FAM-GAAACCCAAACTGAGGTGTAGCAGG-TAMRA. Samples with a cycle
156 threshold value <35 were considered positive based upon validation data using the RNA
157 standards.

158 **Mouse infections, tissue harvest and viral load determination.** Wild-type C57BL/6J mice
159 (Jackson no. 000664) were purchased from the Model Animal Research Center of Nanjing
160 University and housed in animal facilities at the Zhejiang University under
161 specific-pathogen-free condition. For SADS-CoV infections, 6- to 8-week-old female and male
162 mice were inoculated with 5×10^5 $TCID_{50}$ (equal to 6×10^8 genome copies) of SADS-CoV, either
163 per oral infection (p.o.) with 25 μl inoculum (2×10^7 $TCID_{50}$/ml) or intraperitoneal infection (i.p.)

with 200 µl inoculum (2.5×10^6 $TCID_{50}$/ml). For viral load determination in specific tissues, mice were euthanized at 1, 3, 5, 7, 14, 21, and 28 days post-infection (dpi), and tissues were harvested including stomach, duodenum, jejunum, ileum, cecum, colon, mesenteric lymph nodes, spleen, kidney, liver, heart, lung, blood and feces. Tissues were weighed and homogenized in medium (DMEM contained 2% FBS) by bead beating using sterile zirconium oxide beads (Cat# ZrOB20 MidSci). Total RNA was extracted from tissue homogenates and tested by quantitative RT-PCR analysis targeting the SADS-CoV N gene, as described above. Blood samples were collected from the heart and serum was separated for virus-specific antibody detection.

Enzyme-linked immunosorbent assay (ELISA). SADS-CoV virus particles were purified from infected cell culture supernatants by sucrose density gradient centrifugation, and protein concentration was determined by the BCA Protein Assay kit (Beyotime Biotechnology, Shanghai, China). The optimal dilution of antigen was determined by square titration. The IgG antibodies contained in serum at a 1:100 dilution were detected in wells coated with purified SADS-CoV virus particles (6.25 ng/well) as antigen.

Histopathology, immunohistochemistry and immunofluorescence assay for murine spleen. Mice were infected i.p. with SADS-CoV and at 3 dpi, spleens were harvested and fixed in 4% paraformaldehyde for 24 h and embedded in paraffin. Tissue sections were then deparaffinized and rehydrated in three changes of xylene, 15 min each, dehydrated in two changes of pure ethanol for 5 min, followed by rehydration in an ethanol gradient of 85% and 75% ethanol. After washing in distilled water, tissues were subjected to hematoxylin and eosin staining for histopathological examinations.

For antigen retrieval, deparaffinized and rehydrated sections were immersed in sodium citrate antigen retrieval solution (pH 6.0) and maintained at a sub-boiling temperature for 8 min, let stand at 98 °C for 8 min and then incubated again at sub-boiling temperature for 7 min. After allowing to cool to room temperature (RT) and washing three times with PBS (pH 7.4), endogenous peroxidase was blocked by immersion in 3% hydrogen peroxide at RT for 30 min and again washed with PBS. Tissue sections were blocked in 3% BSA at RT for 30 min, then incubated with 1:500 dilution of each primary antibody (anti-dsRNA MAb, anti-SADS-CoV-M pAb or anti-SADS-CoV-AC pAb) overnight at 4 °C. After washing slides three times with PBS (pH 7.4), they were stained with appropriate secondary antibodies labeled with horseradish peroxidase at RT for 50 min. Freshly prepared diaminobenzidine chromogenic reagent was added and counterstained with hematoxylin, then dehydrated and visualized on a light microscope.

Spontaneous fluorescence quenching reagent (Wuhan servicebio technology Co., Ltd, Wuhan, China) was added to the tissue sections and incubated for 5 min after antigen retrieval. The sections were then washed in running water, followed with blocking and antibody staining as described above. In addition, the primary antibody was supplement with a CD11c antibody (Wuhan servicebio technology Co., Ltd, Wuhan, China) at a 1:200 dilution, then stained with appropriate secondary antibodies. Finally, DAPI was added and sections were visualized on a fluorescence microscope; nuclei labeled with DAPI appear blue, positive cells are green by labeling with CD11/c or red by labeling with virus-specific antibody.

Preparation of murine splenocytes and flow cytometry. Mice infected with SADS-CoV were euthanized at 3 dpi, and spleens were removed and placed in 5 ml complete DMEM. After

grinding the excised spleen through a 100-μm cell strainer using the plunger end of a 5-ml syringe, cells were washed with an excess of DMEM and centrifuged at 200 ×g for 5 min. After resuspending cells in 3 ml of red blood cell lysis buffer (Solarbio Life Sciences, Beijing, China) and incubation at RT for 10 min, 5 ml of DMEM was added and cells were passed through another strainer to remove clumps. After centrifugation at 200 ×g for 5 min, the supernatant was discarded and cells were resuspended in 10 ml fresh DMEM for cell counting and viability checks using trypan blue and a hemocytometer.

For flow cytometry, cultured cells were resuspended in Fc Block buffer (containing anti-mouse CD16 Fc Block Antibody at 1:500 dilution) and incubated on ice. Cells in Fc Block buffer were added to 96-well plates at 1×10^6 cells/well. After 30 min incubation, cells were centrifuged at 200 ×g for 10 min, the supernatant was discarded and pellets resuspended in 100 μl Cytofix/Cytoperm solution (Cytofix/Cytoperm Soln Kit; BD Biosciences, San Jose, CA, USA) to fix cells. After incubation on ice for 20 min protected from light, cells were centrifuged at 800 ×g for 5 min at 4 °C, supernatant was removed without disturbing cell pellets and cells were washed twice in 150 μl of 1x Perm/Wash buffer. After addition of 50 μl virus-specific primary antibody (anti-dsRNA MAb, anti-SADS-CoV-N pAb or anti-SADS-CoV-AC pAb) diluted in 1× Perm/Wash buffer with 3% BSA and incubation at 4 °C for 30 min, cells were centrifuged at 200 ×g for 10 min. Cells were washed twice in 150 μl of 1× Perm/Wash buffer followed by staining with appropriate secondary antibodies conjugated to Alexa Fluor 488 (Thermo Fisher Scientific, USA) at 4 °C for 30 min. After centrifuging at 800 ×g for 5 min at 4 °C and washing with 1× Perm/Wash buffer, pellets were resuspended in 0.2 ml FACS buffer and analyzed by flow

cytometry.

Infection of splenocytes *in vitro*. To detect replication of SADS-CoV in mouse splenic cells *in vitro*, splenocytes were extracted from naïve mice, plated in 100- or 35-mm dishes and infected with SADS-CoV at an MOI of 0.1. At 48 hpi, splenocytes were harvested and placed in a 15-ml tube, centrifuged at 200 ×g for 10 min at 4 °C, and analyzed by flow cytometry as described above. Infected mouse splenic cells in 35-mm dishes were detected by immunofluorescence assay with anti-SADS-CoV-N antibodies, and infection supernatants were collected at 0, 12, 24, 36, 48 and 72 hpi for one-step quantitative RT-PCR analysis.

FACS analysis of splenocytes with cell marker staining. Mice infected with SADS-CoV were euthanized at 3 dpi, and splenocytes were prepared for flow cytometry by staining with appropriate antibodies: anti-SADS-CoV-AC following secondary antibodies conjugated to Alexa Fluor 647 (Thermo Fisher Scientific, USA); anti-CD19-FITC (eBioscience, Catalog no.4318813) for B cells; anti-CD4-PE (eBioscience, Catalog no.4329629) for T cells; anti-CD11/c-PE-Cy7 (BD Bioscience, Catalog no.561022) for DCs; and anti-F4/80-PE/Cy5 (Biolegend, Catalog no.123111) for macrophages. Stained cells were resuspended in 0.2 ml FACS buffer and analyzed by flow cytometry.

Production and transduction of S protein-pseudotyped lentiviruses. Pseudovirions with various CoV spike proteins were produced as described previously (19). Briefly, each of the plasmids encoding TGEV, SARS-CoV, MERS-CoV, and mouse hepatitis virus (MHV) S proteins were cotransfected into 293T cells with pLenti-Luc-green fluorescent protein (GFP) and psPAX2 plasmids (kindly provided by Dr. Zhaohui Qian, Chinese Academy of Medical Sciences &

248 Peking Union Medical College) at a molar ratio of 1:1:1 by using polyethylenimine (PEI). The
249 cells were fed with fresh medium in the next 24 h and the supernatant media containing
250 pseudovirions were then collected and centrifuged at 800 ×g for 5 min to remove debris. To
251 quantify S protein-mediated entry of pseudovirions, MDCK cells were seeded at about 25-30%
252 confluency in 24-well plates and transfected with either pAPN-Flag, hDPP4-Flag,
253 mCEACAM1a-Flag, hACE2-GFP (kindly provided by Dr. Zhaohui Qian) (19) or the control
254 backbone vector by using Lipofectamine 3000 (Thermo Fisher). The MDCK cells
255 overexpressing each receptor were inoculated with 500 µl of 1:1 diluted corresponding
256 pseudovirions at 24 h post-transfection. At 40 hpi, cells were lysed at room temperature with 110
257 µl of medium with an equal volume of Steady-Glo (Promega, Madison, WI). The cell lysates
258 were also used to confirm the expression of each receptor by using western blotting.
259 Transduction efficiency was monitored by quantitation of luciferase activity using a Modulus II
260 microplate reader (Turner Biosystems, Sunnyvale, CA). On the other hand, the MDCK cells
261 overexpressing each receptor were inoculated with SADS-CoV (MOI=1) at 24 h
262 post-transfection. IFA was performed to test for SADS-CoV susceptibility using anti-N pAb. The
263 replication competency of SADS-CoV in MDCK cells was further determined by a reverse
264 genetics system. Development of a DNA-launched SADS-CoV (SeACoV) infectious cDNA
265 clone (named pSEA) and rescue of SADS-CoV by transfection of cultured cells with pSEA
266 followed by passaging on Vero cells have been described recently by our lab (16).

267 **Ethics statement.** All animal experiments were performed in strict accordance with the
268 Experimental Animal Ethics Committee of Zhejiang University (approval no. ZJU20170026).

RESULTS

SADS-CoV can infect cell lines originating from various species. Previously, we reported that SADS-CoV was isolated in Vero cells supplemented with trypsin (11). Since exogenous trypsin is essential for propagation of PEDV isolates *in vitro* (20), likely by mediating activation of membrane fusion by S glycoprotein proteolysis (21), we were interesting to know whether it is also required for SADS-CoV growth in cell culture. A total of 24 cell lines originating in various tissues of humans and different animal species were tested for susceptibility to SADS-CoV treated with or without trypsin (Table 1). In brief summary of the results, 21 of the 24 cell lines showed significant susceptibility to SADS-CoV infection, defined by efficient viral replication, antigen expression and the appearance of CPE. The three cell lines that were not infected by SADS-CoV were MDCK, BFK and RAW 264.7.

First, CPE was examined by inverted light microscopy at 48 hpi, and scores are shown in Table 1. As the 293T, NIH/3T3, CHO, BRL-3A and NRK-52E cell lines were sensitive to trypsin, they couldn't be tested for SADS-CoV infection in MMT. Apart from that, CPE was visible in Vero, ST and BRL-3A cell lines without trypsin, and prominent CPE appeared or was enhanced with trypsin in Marc-145, Cos-7, BSC-40, Vero, ST, PK15, LLC-PK1 and BHK-21 cell lines (Table 1).

As some cells did not display CPE after SADS-CoV infection, all cell lines were subsequently tested for viral M protein expression by IFA (Fig. 1), revealing the same range as seen by CPE in the different cell lines (data not shown). Syncytia formation was prominent in

290 Huh-7, Vero and BHK-21 cells, whereas in MDCK, BFK and RAW 264.7 cells the antigen
291 expression was much less prominent than in the other cell lines (Figs. 1A, 1C and 1I). Most cell
292 lines tested showed evidence of productive infection as indicated by expression of the M protein,
293 while the inefficient antigen expression in Marc-145, LLC-PK1 and IPEC-J2 cells suggested
294 only a limited infection.

295 Next, viral load in the culture supernatants was detected over 5 dpi by quantitative RT-PCR
296 (Fig. 2A-2C). A higher mean viral load was detected by qRT-PCR after trypsin treatment in
297 HepG2, HeLa, Marc-145, Cos-7, BSC-40, Vero, LLC-PK1, IPEC-J2, BHK-21 and DF-1 cells.
298 Therefore, trypsin contributes to, but is not essential for SADS-CoV propagation in these cell
299 lines. There was no difference after trypsin treatment in the other cell lines, though Huh-7 and
300 Tb-1 cells had high levels of SADS-CoV RNA regardless of trypsin treatment.

301 The progressive release of infectious SADS-CoV into the culture medium of six
302 representative cell lines infected with SADS-CoV was determined by titration of supernatants in
303 Vero cells (Fig. 2D). Unlike in MDCK cells, SADS-CoV infection of HeLa, Vero, Tb-1,
304 BHK-21 and PK-15 cells was productive, with HeLa cells showing the greatest susceptibility
305 (Fig. 2D).

306 **Wild-type C57BL/6J mice can be infected by SADS-CoV via oral and intraperitoneal**
307 **routes.** With the observation that SADS-CoV could infect diverse rodent cell lines (from mice,
308 rats and hamsters as well as gerbil primary kidney cells), we hypothesized that mice may be
309 susceptible to SADS-CoV. To test this, we inoculated 6- to 8-week-old wild-type B6 mice with
310 5×10^5 $TCID_{50}$ of SADS-CoV by the p.o. or i.p. route and monitored them for 28 days for clinical

311 symptoms. The mice did not succumb to the infection nor did they develop diarrhea or
312 experience weight loss during the incubation period (data not shown).

313 To determine whether SADS-CoV infected the animals asymptomatically, tissue and fecal
314 samples from inoculated mice were collected at 1, 3, 5, 7, 14, 21 and 28 dpi to determine viral
315 growth kinetics and shedding. Analysis of tissue samples by qRT-PCR suggested that
316 SADS-CoV replicated modestly in the stomach early after i.p. or p.o. infection, declining and
317 reaching undetectable levels at 7 or 14 dpi and thereafter (Fig. 3A). A very limited viral
318 replication was observed in each region of the small intestine, with the ileum via i.p. infection
319 showing continuous and decent detectable viral RNA (Fig. 3B). In the large intestine, i.p.
320 infection also resulted in viral RNA loads slightly above the limit of detection at each time point
321 in the ceca, whereas it led to higher viral RNA levels at 1-3 dpi, and much lower viral RNA at
322 21-28 dpi in the colon compared to the p.o. route (Fig. 3C). However, this replication in the large
323 intestine did not translate into higher shedding, as hardly any viral genomes were detected even
324 at 1 dpi in the fecal samples collected from i.p.-infected mice (Fig. 3F). On the contrary,
325 significantly more virus was detected in the feces of p.o.-infected mice at 1 and 3 dpi, indicating
326 that i.p. inoculation does not lead to higher virus shedding.

327 Finally, SADS-CoV replicated more efficiently in the spleen following the i.p. route, with
328 significantly higher viral RNA loads at 21 dpi (Fig. 3D). More importantly, the virus was not
329 cleared from this tissue by 28 dpi in the i.p.-infected group and by 14 dpi in the p.o.-infected
330 group, suggestive of a SADS-CoV prolonged infection in the spleen independent of inoculation
331 route. In contrast to the spleen, only very low levels of viral RNA were detected in the local

lymphoid tissue of mesenteric lymph nodes (MLNs) at 1-3 dpi, and no virus was detectable at later time points (Fig. 3D). We also looked for virus in other extraintestinal sites including the heart, lungs, liver, kidneys and blood, but they were all negative or had extremely low levels (Fig. 3E). IgG antibody levels after 7 days detected by SADS-CoV virion-based ELISA showed that the i.p. route could effectively elicit host immune responses (Fig. 3G).

Splenocytes support SADS-CoV replication. With the mouse infection model described above, our next step was to determine the cell tropism of SADS-CoV *in vivo*. Thus, we performed immunohistochemistry (IHC) on sections of small and large intestine and spleen from mice infected i.p. with 5×10^5 $TCID_{50}$ of SADS-CoV at 3 dpi. A monoclonal antibody against dsRNA was used to identify cells that supported active virus replication, as dsRNA is an intermediate that only exists during intracellular viral replication. SADS-CoV dsRNA signals were observed in the splenic white pulp in the marginal zone on the edge of lymphatic follicles, and in the margins of the periarteriolar lymphocyte sheath (Fig. 4A). Staining of tissue sections from mock-infected mice were used as a control (Fig. 4B). In addition to dsRNA, we also used rabbit pAbs to detect expression of viral structural protein (M) or nonstructural protein (Nsp3-AC). At 3 dpi, anti-M or anti-AC staining was observed in the white pulp around the lymphatic nodules (Fig. 4C), similar to the localization of dsRNA staining (Fig. 4A). Tissue sections from SADS-CoV or mock-infected mice probed with preimmune sera were negative, indicating the specificity of the SADS-CoV antibody. Unfortunately, neither viral proteins (structural or nonstructural) nor dsRNA were detected in the intestine of infected mice, consistent with the detection of only very low levels of viral RNA in these tissues by qRT-PCR

353 (Fig. 3).

354 Next, SADS-CoV infection was quantified in the spleen using flow cytometry. We
355 inoculated B6 wild-type mice with 5×10^5 $TCID_{50}$ of virus either i.p. or p.o., and extracted the
356 bulk immune cells from the spleen of infected animals at 3 dpi. The flow cytometry method was
357 first validated in Vero cells infected with SADS-CoV at an MOI of 0.01 followed by staining
358 with pAb against the N or AC protein at 24 hpi (Fig. 4D). As the anti-AC pAb exhibited optimal
359 intracellular staining for viral signals (Fig. 4D), it was used to determine the percentage of
360 infected splenocytes. Approximately 1.5- and 2.5-fold increase of total splenocytes were positive
361 for virus replication after p.o. and i.p. inoculation, respectively (Fig. 4E, the left panel; Fig. 4F),
362 with a significant increase in the total number of AC-positive splenocytes in i.p.-infected mice
363 compared to p.o. (Fig. 4E, the right panel). This data is consistent with the significantly lower
364 viral loads in the spleen at 1 and 3 dpi in p.o.-inoculated mice (Fig. 3D), suggesting better virus
365 dissemination and replication and escape from mucosal immune clearance.

366 We then evaluated the growth characteristics of SADS-CoV in splenocytes by assessing
367 antigen production and replication kinetics *ex vitro*. Splenocytes were first extracted from naïve
368 mice, plated in 100 mm dishes and infected with 1×10^5 $TCID_{50}$ of SADS-CoV. We observed
369 clusters of infected cells that appeared to have been engulfed by phagocytes (Fig. 4G, the middle
370 panel), and the structural N protein was shown in the cytoplasm of infected cells by confocal
371 microscopy (Fig. 4G, the middle and right panels). The percentage of infected cells was
372 quantified by flow cytometry using anti-AC pAb, revealing that nearly 2-fold increase of the
373 splenocytes were positive for viral signals (Fig. 4H), very similar to the percentage of infection

374 observed *in vivo*. To further characterize the growth kinetic of SADS-CoV in primary
375 splenocytes, cells were infected with 1×10^5 $TCID_{50}$ of SADS-CoV, and culture supernatants
376 were harvested at 0, 12, 24, 48 and 72 hpi. Active viral replication was confirmed, with a 1.5-log
377 time-dependent increase in genomic RNA equivalents, plateauing from 24 to 72 hpi (Fig. 4I).
378 This data suggests that although only ~2% of splenocytes were infected, these cells supported a
379 decent level of viral replication. Together, these results indicate that SADS-CoV productively
380 infects mouse splenocytes.

381 **Splenic DCs support SADS-CoV replication.** Splenocytes were harvested from
382 i.p.-infected mice at 3 dpi, and the extracted cells were co-stained with antibodies against
383 SADS-CoV-AC and each of four cell surface markers (anti-CD19 for B cells; anti-CD4 for T
384 cells; anti-$CD11/c^+$ for DCs and anti-$F4/80^+$ for macrophages) using flow cytometry (Fig. 5A).
385 The percentage of infected $CD11/c^+$ cells was significantly higher than the other cell subgroups,
386 indicating that DCs are the major targets of SADS-CoV infection in the spleen.

387 The phenotype was further confirmed by double-staining IFA with anti-dsRNA, anti-M or
388 anti-AC antibody plus anti-$CD11/c^+$ in splenic sections. As expected, dsRNA staining
389 overlapped with the CD11/c surface marker on the edges of lymphatic follicles (Fig. 5B),
390 whereas no viral signals were seen in the mock-infected control (Fig. 5C). Similar patterns of
391 co-staining were detected by M and AC antibodies (Fig. 5D). To gain insight into the relative
392 quantity of DCs compared to other undefined target cells, cells positive for dsRNA and CD11/c
393 were counted in 10-15 different microscope fields of spleens from 3 infected mice (Fig. 5E),
394 showing that 61.76% of SADS-CoV-infected cells were DCs (Fig. 5F).

SADS-CoV does not utilize known CoV protein receptors for cellular entry. To our knowledge, these results reveal the most extensive cell tropism among known CoVs, suggesting the functional receptor(s) for SADS-CoV is likely to be a very common molecule. In order to test this hypothesis, it was first necessary to find a cell line that was refractory to infection only at the internalization step. MDCK cells, which showed undetectable virus production in early infection tests (Fig. 1 and Fig. 2), were chosen as a potential candidate. There are four known types of functional CoV protein receptors, including angiotensin converting enzyme 2 (ACE2) for SARS-CoV (22), dipeptidyl peptidase 4 (DPP4) for MERS-CoV (23), aminopeptidase N (APN) for TGEV (24) and PDCoV (25, 26), and mouse carcinoembryonic antigen-related cell adhesion molecule 1a (mCEACAM1a) for MHV (27). To test whether one of these molecules serves as the SADS-CoV receptor, we attempted to inoculate non-susceptible MDCK cells overexpressing porcine APN, human DPP4, mouse CEACAM1a, or human ACE2 with SADS-CoV, but none of them allowed infection as staining with anti-SADS-CoV-N pAb was negative (Fig. 6A). Meanwhile, the expression of each receptor in MDCK cells was confirmed by IFA (Fig. 6A) and western blot analysis (Fig. 6B) using antibodies against the tags fused to the receptors. As positive controls, we confirmed that lentiviruses pseudotyped with TGEV, SARS-CoV, MERS-CoV or MHV spike (i.e., pseudoviruses) efficiently entered MDCK cells exogenously expressing the respective receptors (Fig. 6C).

Next, we demonstrated that MDCK cells can confer SADS-CoV replication competency by transfection of a SADS-CoV/SeACoV infectious cDNA clone established recently (16), as simultaneous expression of Nsp3-AC and N proteins were clearly detected by IFA (Fig. 6D).

Moreover, passaging of supernatants from pSEA-transfected MDCK cells onto fresh Vero cells resulted in progeny SADS-CoV infection, as evidenced by expression of the N protein (Fig. 6E), indicating that MDCK cells can also support infectious SADS-CoV production without cell-to-cell spread. Therefore, SADS-CoV apparently does not utilize any of the known CoV receptors for cellular entry. The same conclusion was reached using HeLa cells overexpressing each of the four classical CoV receptors followed by SADS-CoV inoculation by Zhou et al (14); however, the HeLa cell line itself was most susceptible to SADS-CoV infection in the present study (Fig. 2D).

DISCUSSION

In order to assess the potential species barriers of SADS-CoV infection, a cell line susceptibility study was first conducted using 24 different cell lines. As SADS-CoV probably originated from a bat SADSr-CoV (14) derived from HKU2-CoV identified in *Rhinolophus sinicus* (Chinese horseshoe bats) (12), we commenced testing viral susceptibility in two available bat cell lines, BFK from *Myotis daubentonii* (18) and Tb-1 from *Tadarida brasiliensis*. Although BFK cells did not support SADS-CoV replication, it replicated efficiently in Tb-1 cells (Fig. 1A and Fig. 2), suggesting that other bat species in addition to horseshoe bats are likely susceptible to SADS-CoV infection.

Interestingly, SADS-CoV protein expression was detected in almost all of the rodent cells (hamster, gerbil, mouse and rat) including BHK-21, which is not susceptible to other known human CoVs such as SARS-CoV and MERS-CoV (28, 29) as well as three swine enteric CoVs,

437 PEDV, PDCoV and TGEV (25). Given the fact that SADS-CoV infects both primary and
438 passaged or primary cell lines originating from rodents, we hypothesized that rodents may be
439 susceptible to SADS-CoV infection. To explore this possibility, we challenged wild-type B6
440 mice with SADS-CoV by two different inoculation routes.

441 The challenged animals neither succumbed to infection nor manifested any signs of
442 gastroenteritis. In fact, experimental infection of neonatal piglets with a higher dose of purified
443 SADS-CoV in our laboratory only resulted in mild diarrheal signs or subclinical infection (11).
444 Also, there was a lack of robust viral replication in the intestines during infection, and no tissue
445 damage was detected throughout the intestines (Fig. 3B and 3C), reflecting the suboptimal
446 infection by SADS-CoV in immunocompetent wild-type mice. On the contrary, the virus had
447 more efficient replication within the spleen, reflected by a continuous detection of viral genomic
448 RNA in the immune cells at all time points over a 28-day period (Fig. 3D). The phenotype was
449 also consistent with the replication kinetics in extracted splenocytes *in vitro*, in which viral
450 genomic RNA peaked and plateaued at 72 hpi (Fig. 4G and 4I). This data collectively led to
451 speculation that SADS-CoV favors splenic cells over other tissues. The most logical explanation
452 for these tissue-specific discrepancies in virus replication is: i) target cells are more concentrated
453 in the spleen and more sporadic in the intestine; or ii) splenic immune cells have enhanced
454 expression of the unknown receptor(s) over intestinal cells. The animals were more susceptible
455 to i.p. infection, resulting in higher virus replication in the distal section of the small intestine,
456 large intestine and spleen, and perhaps a delayed clearance of viral infection in the cecum (Fig.
457 3B to 3E), suggesting the important role of mucosal immunity for controlling early infection in

458 SADS-CoV in mice. It should be note that mice (C57BL/6J mice in this study) may not be the
459 optimal rodent species for SADS-CoV infection, as wild rats are more commonly seen in
460 Chinese pig farms. In addition, other transmission routes may be considered. Recently, PDCoV
461 has been shown to possibly spread via the respiratory route in addition to fecal-oral transmission
462 (30). Therefore, it will be interesting to try intranasal route for inoculation in rats or the other
463 rodent species to mimic SADS-CoV natural transmission in future studies.

464 More interestingly, we identified DCs to be the precise cell population that supported
465 SADS-CoV replication (Fig. 5). There have been a few reports of immune cell tropism for CoVs.
466 Macrophages are susceptible to MHV infection, representing the largest group of innate immune
467 cells that infiltrate the central nervous system after infection with neurotropic MHV strains (31).
468 In addition, based on the fact that SARS-CoV spike-pseudotyped HIV-based vectors can
469 efficiently transduce human DCs, Kobinger *et al*. hypothesized that SARS-CoV infection in
470 immature DCs contributes to viral pathogenesis (32). Yang *et al*. demonstrated that SARS-CoV
471 can infect myeloid DCs via S glycoprotein-associated cell entry, and DC infection mediated viral
472 transmission to other cells *in vivo* (33). These previous evidences support our present results,
473 showing that SADS-CoV can efficiently replicate in DCs.

474 Furthermore, this study gives us a novel inspiration that rodents may potentially serve as
475 susceptible hosts for SADS-CoV in addition to bats and pigs. Of note, the species *Rhinolophus*
476 *bat α-CoV HKU2*, including SADS-CoV, possesses unique S genes closely related to the
477 betacoronavirus (β-CoV), in a manner similar to some globally distributed rodent α-CoVs (11, 34,
478 35), implying an unknown evolutionary connection between the bat α-CoV HKU2 and rodents

479 α-CoVs. In the field conditions of China, direct contact between pigs and flying bats is a low
480 probability; however, rodents (especially rats) are frequently visible in the swine industry,
481 causing great nuisance due to feed loss. It is possible that as bats prey on insects near pig
482 facilities, they leave feces containing HKU2-like CoVs that contaminate pig feed, which is then
483 eaten by pig and rodents that subsequently become carriers of SADS-CoV. Rats and mice are
484 increasingly implicated as external vectors for a wide range of different pig pathogens, such as *L.*
485 *intracellularis* (36). Rodents not only spread pathogens, but also harm the practitioners of the
486 swine industry, as they are thought to be the major source of leptospirosis in pigs and piggery
487 workers (37). Future study on identifying SADS-CoV-positive samples in rodents near pig farms
488 are warranted to test this hypothesis.

489 In addition to rodents, we also measured the SADS-CoV susceptibility of cell lines from
490 humans, monkeys, chickens and dogs, revealing a remarkably broad spectrum of tropism (Table
491 1 and Fig. 1). As for the ability of SADS-CoV to grow efficiently in human cell lines, we should
492 not underestimate the risk that this bat-origin CoV may 'jump' from pigs to humans. It is
493 noteworthy that camel workers with high rates of exposure to camel nasal and oral secretions had
494 evidence of MERS-CoV infection (38). Considering that SARS-CoV and MERS-CoV originated
495 from bats and spread from one species to another through intermediate hosts (civets and camels,
496 respectively), SADS-CoV may pose a similar risk to human health through transmission from
497 pigs or other susceptible hosts.

498 The cell susceptibility study and testing of overexpression of four known CoV receptors in
499 non-susceptible MDCK cells (Fig. 6) demonstrated that SADS-CoV might use a new receptor

molecule that is conserved in bats, pigs, rodents, chickens, monkeys and humans, indicating a low barrier to cross-species transmission. This is in line with the unusual feature of SADS-CoV's apparently broad species tropism.

In summary, these results provide important insights into the ecology of this bat-origin CoV, highlighting the possibility of its jumping interspecies barriers and the potential role of rodents as susceptible hosts in the field. Identification of the unknown SADS-CoV cellular receptor and further surveillance of other animal populations are needed to fully understand the biology of SADS-CoV.

ACKNOWLEDGMENTS

This work was supported by the National Key Research and Development Program of China (2016YFD0500102), the National Natural Science Foundation of China (31872488) and the Fundamental Research Funds for the Central Universities of China (2019FZA6014). The professional editing service NB Revisions was used for technical preparation of the text prior to submission.

References

1. **Graham RL, Baric RS.** 2010. Recombination, reservoirs, and the modular spike: mechanisms of coronavirus cross-species transmission. J Virol **84:**3134-3146.

2. **van Boheemen S, de Graaf M, Lauber C, Bestebroer TM, Raj VS, Zaki AM, Osterhaus AD, Haagmans BL, Gorbalenya AE, Snijder EJ, Fouchier RA.** 2012. Genomic characterization of a newly

discovered coronavirus associated with acute respiratory distress syndrome in humans. MBio **3:**e00473-00412.

3. **Soma T, Saito N, Kawaguchi M, Sasai K.** 2018. Feline coronavirus antibody titer in cerebrospinal fluid from cats with neurological signs. J Vet Med Sci **80:**59-62.

4. **Huang YW, Dickerman AW, Pineyro P, Li L, Fang L, Kiehne R, Opriessnig T, Meng XJ.** 2013. Origin, evolution, and genotyping of emergent porcine epidemic diarrhea virus strains in the United States. MBio **4:**e00737-00713.

5. **Lu G, Wang Q, Gao GF.** 2015. Bat-to-human: spike features determining 'host jump' of coronaviruses SARS-CoV, MERS-CoV, and beyond. Trends Microbiol **23:**468-478.

6. **Ksiazek TG, Erdman D, Goldsmith CS, Zaki SR, Peret T, Emery S, Tong S, Urbani C, Comer JA, Lim W, Rollin PE, Dowell SF, Ling AE, Humphrey CD, Shieh WJ, Guarner J, Paddock CD, Rota P, Fields B, DeRisi J, Yang JY, Cox N, Hughes JM, LeDuc JW, Bellini WJ, Anderson LJ, Group SW.** 2003. A novel coronavirus associated with severe acute respiratory syndrome. N Engl J Med **348:**1953-1966.

7. **Drexler JF, Corman VM, Drosten C.** 2014. Ecology, evolution and classification of bat coronaviruses in the aftermath of SARS. Antiviral Res **101:**45-56.

8. **Chan JF, Lau SK, To KK, Cheng VC, Woo PC, Yuen KY.** 2015. Middle East respiratory syndrome coronavirus: another zoonotic betacoronavirus causing SARS-like disease. Clin Microbiol Rev **28:**465-522.

9. **Yin Y, Wunderink RG.** 2018. MERS, SARS and other coronaviruses as causes of pneumonia. Respirology **23:**130-137.

10. **Hulswit RJ, de Haan CA, Bosch BJ.** 2016. Coronavirus Spike Protein and Tropism Changes. Adv Virus

Res **96:**29-57.

11. **Pan Y, Tian X, Qin P, Wang B, Zhao P, Yang YL, Wang L, Wang D, Song Y, Zhang X, Huang YW.** 2017. Discovery of a novel swine enteric alphacoronavirus (SeACoV) in southern China. Vet Microbiol **211:**15-21.

12. **Lau SK, Woo PC, Li KS, Huang Y, Wang M, Lam CS, Xu H, Guo R, Chan KH, Zheng BJ, Yuen KY.** 2007. Complete genome sequence of bat coronavirus HKU2 from Chinese horseshoe bats revealed a much smaller spike gene with a different evolutionary lineage from the rest of the genome. Virology **367:**428-439.

13. **Gong L, Li J, Zhou Q, Xu Z, Chen L, Zhang Y, Xue C, Wen Z, Cao Y.** 2017. A New Bat-HKU2-like Coronavirus in Swine, China, 2017. Emerg Infect Dis **23:**1607-1609.

14. **Zhou P, Fan H, Lan T, Yang XL, Shi WF, Zhang W, Zhu Y, Zhang YW, Xie QM, Mani S, Zheng XS, Li B, Li JM, Guo H, Pei GQ, An XP, Chen JW, Zhou L, Mai KJ, Wu ZX, Li D, Anderson DE, Zhang LB, Li SY, Mi ZQ, He TT, Cong F, Guo PJ, Huang R, Luo Y, Liu XL, Chen J, Huang Y, Sun Q, Zhang XL, Wang YY, Xing SZ, Chen YS, Sun Y, Li J, Daszak P, Wang LF, Shi ZL, Tong YG, Ma JY.** 2018. Fatal swine acute diarrhoea syndrome caused by an HKU2-related coronavirus of bat origin. Nature **556:**255-258.

15. **Wang L, Su S, Bi Y, Wong G, Gao GF.** 2018. Bat-Origin Coronaviruses Expand Their Host Range to Pigs. Trends Microbiol **26:**466-470.

16. **Yang YL, Liang QZ, Xu SY, Mazing E, Xu GH, Peng L, Qin P, Wang B, Huang YW.** 2019. Characterization of a novel bat-HKU2-like swine enteric alphacoronavirus (SeACoV) infection in cultured cells and development of a SeACoV infectious clone. Virology **536:**110-118.

17. **Ji CM, Wang B, Zhou J, Huang YW.** 2018. Aminopeptidase-N-independent entry of porcine epidemic diarrhea virus into Vero or porcine small intestine epithelial cells. Virology **517:**16-23.

18. **He B, Yang F, Yang W, Zhang Y, Feng Y, Zhou J, Xie J, Feng Y, Bao X, Guo H, Li Y, Xia L, Li N, Matthijnssens J, Zhang H, Tu C.** 2013. Characterization of a novel G3P[3] rotavirus isolated from a lesser horseshoe bat: a distant relative of feline/canine rotaviruses. J Virol **87:**12357-12366.

19. **Ou XY, Zheng WL, Shan YW, Mu ZX, Dominguez SR, Holmes KV, Qian ZH.** 2016. Identification of the Fusion Peptide-Containing Region in Betacoronavirus Spike Glycoproteins. Journal of Virology **90:**5586-5600.

20. **Hofmann M, Wyler R.** 1988. Propagation of the virus of porcine epidemic diarrhea in cell culture. J Clin Microbiol **26:**2235-2239.

21. **Wicht O, Li W, Willems L, Meuleman TJ, Wubbolts RW, van Kuppeveld FJ, Rottier PJ, Bosch BJ.** 2014. Proteolytic activation of the porcine epidemic diarrhea coronavirus spike fusion protein by trypsin in cell culture. J Virol **88:**7952-7961.

22. **Li W, Moore MJ, Vasilieva N, Sui J, Wong SK, Berne MA, Somasundaran M, Sullivan JL, Luzuriaga K, Greenough TC, Choe H, Farzan M.** 2003. Angiotensin-converting enzyme 2 is a functional receptor for the SARS coronavirus. Nature **426:**450-454.

23. **Raj VS, Mou H, Smits SL, Dekkers DH, Muller MA, Dijkman R, Muth D, Demmers JA, Zaki A, Fouchier RA, Thiel V, Drosten C, Rottier PJ, Osterhaus AD, Bosch BJ, Haagmans BL.** 2013. Dipeptidyl peptidase 4 is a functional receptor for the emerging human coronavirus-EMC. Nature **495:**251-254.

24. **Delmas B, Gelfi J, L'Haridon R, Vogel LK, Sjostrom H, Noren O, Laude H.** 1992. Aminopeptidase N

is a major receptor for the entero-pathogenic coronavirus TGEV. Nature **357:**417-420.

25. **Wang B, Liu Y, Ji CM, Yang YL, Liang QZ, Zhao P, Xu LD, Lei XM, Luo WT, Qin P, Zhou J, Huang YW.** 2018. Porcine deltacoronavirus engages the transmissible gastroenteritis virus functional receptor porcine aminopeptidase N for infectious cellular entry. J Virol **92:**e00318-00318.

26. **Li W, Hulswit RJG, Kenney SP, Widjaja I, Jung K, Alhamo MA, van Dieren B, van Kuppeveld FJM, Saif LJ, Bosch BJ.** 2018. Broad receptor engagement of an emerging global coronavirus may potentiate its diverse cross-species transmissibility. Proc Natl Acad Sci U S A **115:**E5135-E5143.

27. **Williams RK, Jiang GS, Holmes KV.** 1991. Receptor for mouse hepatitis virus is a member of the carcinoembryonic antigen family of glycoproteins. Proc Natl Acad Sci U S A **88:**5533-5536.

28. **Chan JF, Chan KH, Choi GK, To KK, Tse H, Cai JP, Yeung ML, Cheng VC, Chen H, Che XY, Lau SK, Woo PC, Yuen KY.** 2013. Differential cell line susceptibility to the emerging novel human betacoronavirus 2c EMC/2012: implications for disease pathogenesis and clinical manifestation. J Infect Dis **207:**1743-1752.

29. **Muller MA, Raj VS, Muth D, Meyer B, Kallies S, Smits SL, Wollny R, Bestebroer TM, Specht S, Suliman T, Zimmermann K, Binger T, Eckerle I, Tschapka M, Zaki AM, Osterhaus AD, Fouchier RA, Haagmans BL, Drosten C.** 2012. Human coronavirus EMC does not require the SARS-coronavirus receptor and maintains broad replicative capability in mammalian cell lines. MBio **3:**e00515-00512.

30. **Woo PC, Lau SK, Tsang CC, Lau CC, Wong PC, Chow FW, Fong JY, Yuen KY.** 2017. Coronavirus HKU15 in respiratory tract of pigs and first discovery of coronavirus quasispecies in 5'-untranslated region. Emerg Microbes Infect **6:**e53.

31. **Mazaleuskaya L, Veltrop R, Ikpeze N, Martin-Garcia J, Navas-Martin S.** 2012. Protective role of

Toll-like Receptor 3-induced type I interferon in murine coronavirus infection of macrophages. Viruses **4:**901-923.

32. **Kobinger GP, Limberis MP, Somanathan S, Schumer G, Bell P, Wilson JM.** 2007. Human immunodeficiency viral vector pseudotyped with the spike envelope of severe acute respiratory syndrome coronavirus transduces human airway epithelial cells and dendritic cells. Hum Gene Ther **18:**413-422.

33. **Yang ZY, Huang Y, Ganesh L, Leung K, Kong WP, Schwartz O, Subbarao K, Nabel GJ.** 2004. pH-dependent entry of severe acute respiratory syndrome coronavirus is mediated by the spike glycoprotein and enhanced by dendritic cell transfer through DC-SIGN. J Virol **78:**5642-5650.

34. **Tsoleridis T, Chappell JG, Onianwa O, Marston DA, Fooks AR, Monchatre-Leroy E, Umhang G, Muller MA, Drexler JF, Drosten C, Tarlinton RE, McClure CP, Holmes EC, Ball JK.** 2019. Shared Common Ancestry of Rodent Alphacoronaviruses Sampled Globally. Viruses **11**.

35. **Wang W, Lin XD, Guo WP, Zhou RH, Wang MR, Wang CQ, Ge S, Mei SH, Li MH, Shi M, Holmes EC, Zhang YZ.** 2015. Discovery, diversity and evolution of novel coronaviruses sampled from rodents in China. Virology **474:**19-27.

36. **Collins AM, Fell S, Pearson H, Toribio JA.** 2011. Colonisation and shedding of Lawsonia intracellularis in experimentally inoculated rodents and in wild rodents on pig farms. Vet Microbiol **150:**384-388.

37. **Everard CO, Ferdinand GA, Butcher LV, Everard JD.** 1989. Leptospirosis in piggery workers on Trinidad. J Trop Med Hyg **92:**253-258.

38. **Alshukairi AN, Zheng J, Zhao J, Nehdi A, Baharoon SA, Layqah L, Bokhari A, Al Johani SM, Samman N, Boudjelal M, Ten Eyck P, Al-Mozaini MA, Zhao J, Perlman S, Alagaili AN.** 2018. High Prevalence of MERS-CoV Infection in Camel Workers in Saudi Arabia. MBio **9:**e01985-01918.

626

627 ## FIGURE LEGENDS

628

629 **Figure 1. Immunofluorescence assay showing susceptibility of different cell lines to**
630 **SADS-CoV infection.** Immunofluorescence assay of cells infected with SADS-CoV at an
631 MOI=0.01 was performed using rabbit anti-SADS-CoV-M polyclonal Ab (200× magnification)
632 and Alexa Fluor 488-conjugated anti-rabbit IgG as secondary antibody, with DAPI for
633 visualization of cell nuclei. Mock-infected cells were treated with the same procedures as
634 appropriate. Cells were tested from different species of origin, including: **(A)** Bats (BFK and
635 Tb-1); **(B)** Hamsters (CHO and BHK-21); **(C)** Mice (NIH/3T3 and RAW264.7); **(D)** Rats
636 (BRL-3A and NRK-52E); **(E)** Humans (Huh-7, HepG2, 293T, A549, and HeLa); **(F)** Monkeys
637 (Marc-145, Cos-7, BSC-40, and Vero); **(G)** Pigs (ST, PK15, LLC-PK1, and IPEC-J2); **(H)**
638 Chickens (DF-1); **(I)** Dogs (MDCK); and **(J)** Gerbil primary kidney cells.

639

640 **Figure 2. Growth of SADS-CoV in different cell lines through five days post-infection.** To
641 determine the effect of trypsin on SADS-CoV infection, each cell line was infected in three
642 conditions: **(A)** "No trypsin" treatment: inoculated with SADS-CoV diluted in maintenance
643 medium (MM) for 2 h, and subsequently replaced with MM; **(B)** "Pre-trypsin" treatment:
644 inoculated with SADS-CoV diluted in MM containing 5 μg/ml trypsin (MMT) for 2 h, and
645 subsequently replaced with MM; and **(C)** "Double-trypsin" treatment: inoculated with
646 SADS-CoV in MMT, and subsequently replaced with MMT. Infection supernatants were

collected at 12, 24, 36, 48, 72 and 120 hpi for viral load detection by a qRT-PCR assay targeting the viral N gene. Data is expressed as the mean viral load (log_{10} copies/µl) ± standard deviation (SD), and all experiments were performed in triplicate. The 293T, CHO, BRL-3A and NRK-52E cell lines did not survive in the presence of trypsin. **(D)** Infectious titers ($TCID_{50}$/ml) of SADS-CoV secreted from HeLa, Vero, Tb-1, BHK-21 PK-15 and MDCK cells were determined on Vero cells.

Figure 3. SADS-CoV infection of mice. C57BL/6J WT mouse were infected per orally (p.o; black) or intraperitoneally (i.p; red) with 5×10^5 $TCID_{50}$ of purified SADS-CoV. Viral loads in different tissue samples including **(A)** stomach, **(B)** small intestinal segments, **(C)** large intestinal segments, **(D)** lymphoid tissues, **(E)** the other organs (liver, kidney, heart and lung) and **(F)** feces collected at 1, 3, 5, 7, 14, 21, and 28 days post-infection (dpi) were determined by qRT-PCR; MLN: Mesenteric lymph nodes. Data are from three independent experiments, and each symbol represents titers from an individual sample (*: $p<0.05$). The limit of detection was 1×10^2 genome copies/mg. **(G)** SADS-CoV IgG antibodies were detected in serum samples collected at euthanasia, using an ELISA based on purified SADS-CoV virus particles.

Figure 4. SADS-CoV replication in mouse splenocytes. (A) Hematoxylin & eosin staining (HE) and immunohistochemistry (IHC) were performed on sections of spleen from intraperitoneally infected mice and **(B)** Mock-infected mice at 3 dpi, using anti-dsRNA antibodies to identify splenic cells that support active virus replication. **(C)** SADS-CoV infection could also be

668 detected by IHC using SADS-CoV nonstructural protein antibody (anti-AC) and structural
669 protein antibody (anti-M). Scale bars=50 μm, except for magnified fields shown on the right side,
670 with scale bars=10 μm. **(D)** SADS-CoV antibody validation in Vero cells for developing the flow
671 cytometry assay. Flow cytometry plots of Vero cells infected with SADS-CoV (MOI=0.1) at 24
672 hpi, staining with anti-N or anti-AC. **(E)** Flow cytometry detection of Nsp3-AC antigens of
673 SADS-CoV in splenocytes from infected mice using anti-AC antibody at 3 dpi. The data are
674 presented as the fold-increase in staining splenocytes from infected mice relative to the
675 mock-infected group for statistical purposes (left panel); *: $p<0.05$. **(F)** Representative
676 FACS plots of panel (E). The solid-line frame gated anti-AC positive splenocytes from p.o. or i.p.
677 inoculated mice. The plot of mock-infected cells stained with secondary antibody only was also
678 shown. **(G)** Isolated mouse splenocytes were infected with SADS-CoV at an MOI=1, and
679 SADS-CoV N protein expression was detected by IFA with anti-N antibody. **(H)** Flow cytometry
680 detection of nonstructural protein antigens of SADS-CoV in infected splenocytes at 48 hpi using
681 anti-AC antibody. The data are presented as the fold-increase in staining cells relative to the
682 mock-infected cells for statistical purposes (left panel); *: $p<0.05$. **(I)** Growth of SADS-CoV in
683 *ex vivo* splenocytes was monitored over 72 hpi by qRT-PCR targeting the SADS-CoV N gene.
684
685 **Figure 5. SADS-CoV infection of dendritic cells in the spleen of mice inoculated via i.p.**
686 **route. (A)** Splenocytes were extracted from infected mice at 3 dpi, and flow cytometry was used
687 to detect nonstructural antigen AC of SADS-CoV with immune cell markers on splenocytes
688 including B cells ($CD19^+$), T cells ($CD4^+$), macrophages ($F4/80^+$), and dendritic cells (DCs,

689 CD11c^{+}). The data are presented as the fold-increase in positive staining cells from infected mice
690 relative to the mock-infected cells for statistical purposes; ***: p<0.001. **(B)**
691 Immunofluorescence assay of SADS-CoV dsRNA and DC marker CD11c in sections of spleen
692 from intraperitoneally (i.p.) infected mice and **(C)** mock-infected mice at 3 dpi. **(D)** SADS-CoV
693 infection could also be detected by IFA using anti-AC and anti-M antibodies. **(E)** The numbers of
694 SADS-CoV-positive DCs in i.p.-infected mice were counted and averaged from 10-15 different
695 visual fields, and **(F)** the proportion of DCs in infected cells was presented with a Venn diagram.
696 Scale bars = 50 μm, except for magnified fields shown on the right side, with scale bars =10 μm.
697
698 **Figure 6. SADS-CoV utilizes an unknown receptor for cellular entry. (A)** MDCK cells
699 overexpressing each of the four known CoV receptors fused with detectable tags (pAPN-Flag,
700 hDPP4-Flag, mCEACAM1a-Flag, or hACE2-GFP) did not confer SADS-CoV infection at 24 h
701 post-transfection of the expression plasmids. At 48 h, SADS-CoV-inoculated cells transfected
702 with pAPN-Flag, hDPP4-Flag, or mCEACAM1a-Flag were co-stained with a mouse anti-FLAG
703 MAb and a rabbit anti-SADS-CoV-N pAb. Alexa Fluor 488-conjugated anti-mouse IgG and
704 Alexa Fluor 594-conjugated anti-rabbit IgG were co-stained for secondary antibody detection,
705 followed by DAPI incubation. For challenged cells transfected with hACE2-GFP,
706 anti-SADS-CoV-N pAb and Alexa Fluor 594-conjugated anti-rabbit IgG were used;
707 magnification=200×. **(B)** Western blot analysis also confirmed the expression of CoV receptors
708 in transfected MDCK cells. **(C)** TGEV-, SARS-CoV-, MERS-CoV- or MHV-spike-mediated
709 pseudovirus entry into MDCK cells overexpressing the corresponding receptor. The pseudovirus

entry efficiency was characterized as luciferase activity accompanying the entry. Cells transfected with the empty backbone vector were used as controls. **(D)** Rescue of SADS-CoV in MDCK cells transfected with a SeACoV infectious cDNA clone. Detection of expression of Nsp3-AC and N proteins of SADS-CoV was conducted at 72 h post-transfection by co-staining with a rabbit anti-AC pAb and a mouse anti-N pAb (magnification = 200×). **(E)** Infection of fresh Vero cells with progeny SADS-CoV rescued in MDCK cells. The expression of SADS-CoV N protein was detected by staining with anti-N pAb at 36 hpi.

Journal of Virology

Table 1. Summary of human and animal cell lines and their susceptibility to SADS-CoV infection as determined by cytopathic effect (CPE) and IFA.

Cell lines			Without Trypsin		With Trypsin	
Species and/or tissue origin	Name	ATCC® Number	IFA	CPE	IFA	CPE
Human						
Hepatocellular carcinoma	Huh-7	N/A	++	-	++	-
Hepatocellular carcinoma	HepG2/C3A	HB-8065	+	-	++	-
Embryonic kidney	293T	CRL-11268	+	-	N/D	N/D
Lung carcinoma	A549	CCL-185EMT	+	-	++	-
Cervix adenocarcinoma	HeLa	CCL-2	+	-	+	-
Monkey						
African green monkey kidney	Marc-145	N/A	+	-	++	+
African green monkey kidney	Cos-7	CRL-1651	++	-	+++	++
African green monkey kidney	BSC-40	CRL-2761	++	-	+++	++
African green monkey kidney	Vero	CRL-1586	++	+	+++	+++
Swine						
Testis	ST	CRL-1746	+	+	++	++
Kidney	PK15	CCL-33	+	-	++	+
Kidney	LLC-PK1	CL-101	+	-	++	+
Small intestinal epithelium	IPEC-J2	N/A	+	-	+	-
Bat						
Myotis petax, fetal kidney	BFK	N/A	-	-	-	-
Tadarida brasiliensis, lung	Tb-1	CCL-88	+	-	++	-
Canine						
Kidney	MDCK	CCL-34	-	-	-	-
Mouse						
Embryo fibroblasts	NIH/3T3	CRL-1658	+	-	N/D	N/D
Monocyte/macrophage	RAW 264.7	TIB-71	-	-	-	-
Hamster						
Syrian golden hamster, kidney	BHK-21	CCL-10	+	-	+++	+
Chinese hamster, ovary	CHO	CCL-61	+	-	N/D	N/D
Rat						
Liver	BRL 3A	CRL-1442	++	+	N/D	N/D
Kidney	NRK-52E	CRL-1571	+	-	N/D	N/D
Gerbil						
Primary kidney cells		N/A	++	-	N/D	N/D
Chicken						
Embryo fibroblasts	DF-1	CRL-12203	+	-	N/D	N/D

Degree of infection as determined by IFA or CPE (-: No infection or obvious lesion≤1%; +: ≤25%; ++: ≤50%; +++: ≤75%; ++++: ≤100%);

N/A: Not available; N/D: Not detected due to cell sensitivity to trypsin.

Figure 1

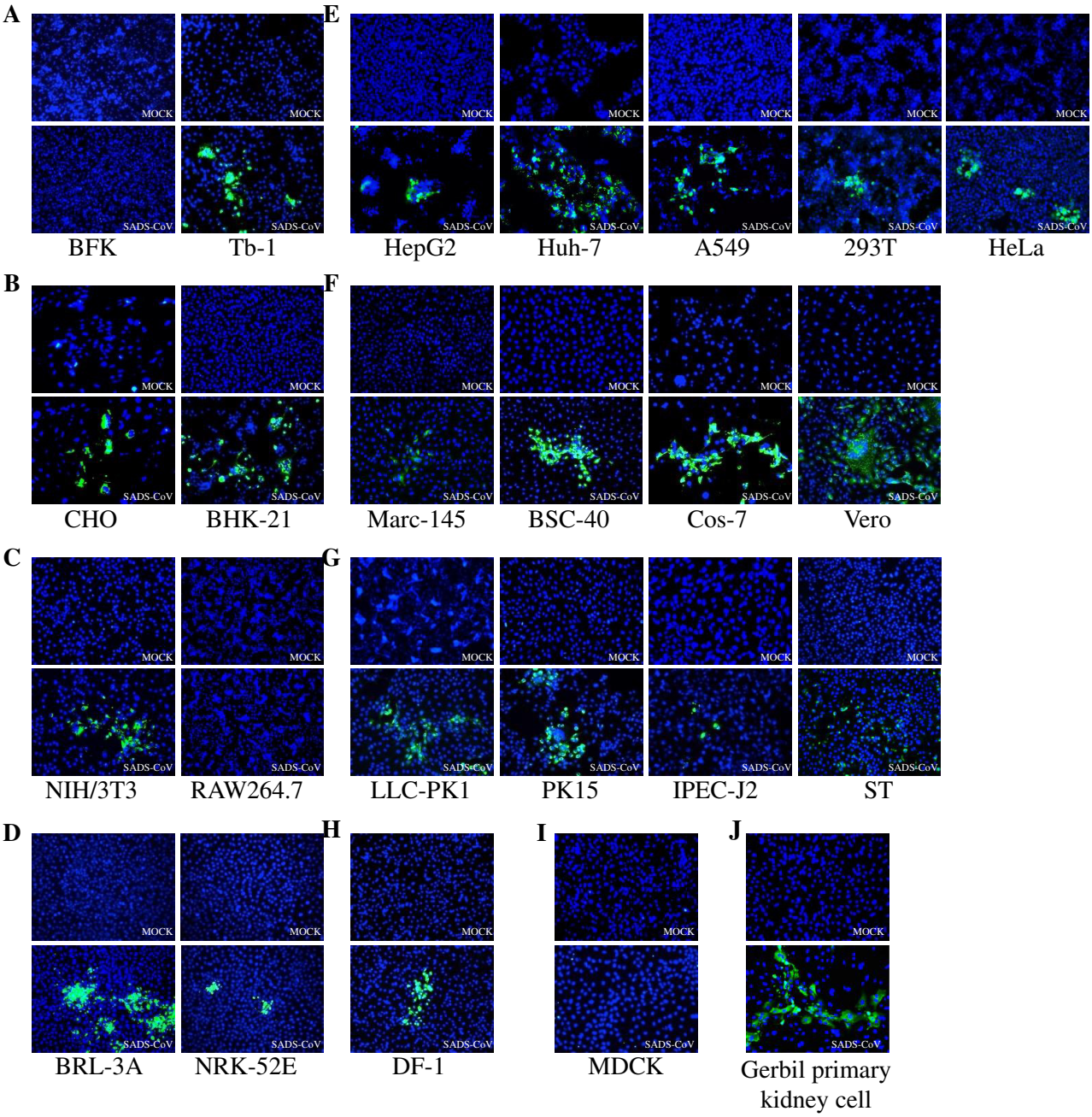

Figure 2

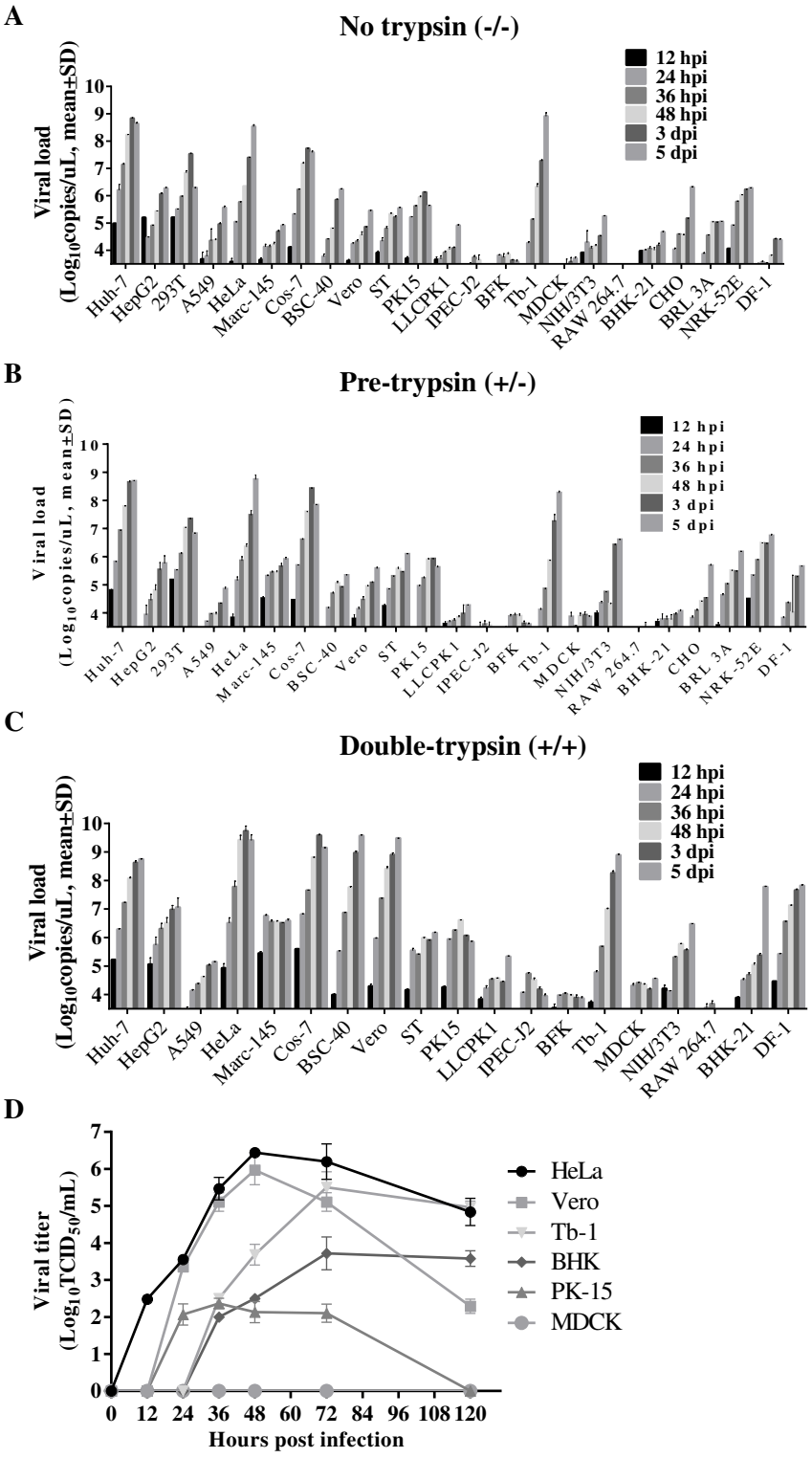

Figure 3

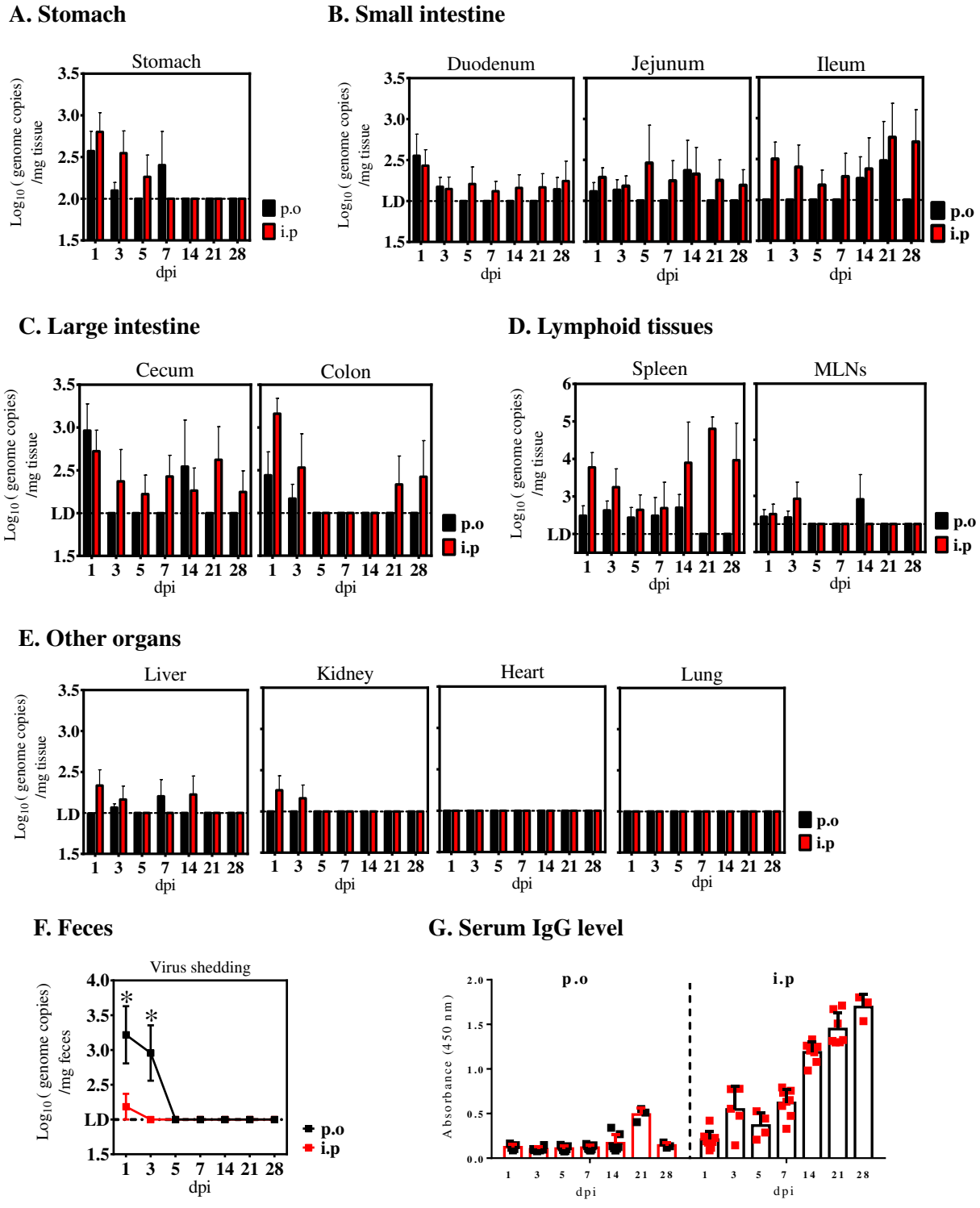

Figure 4

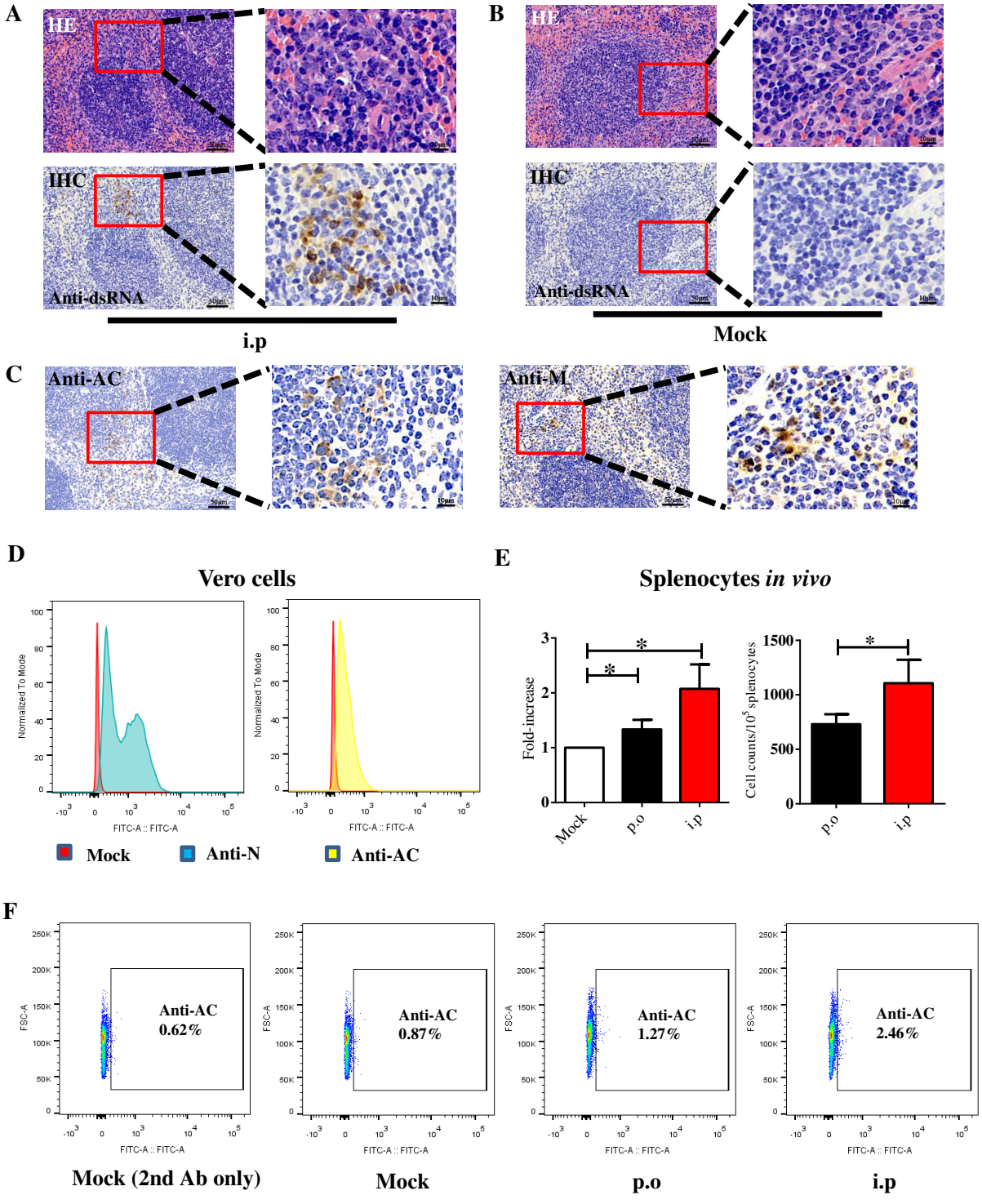

Figure 4 (continued)

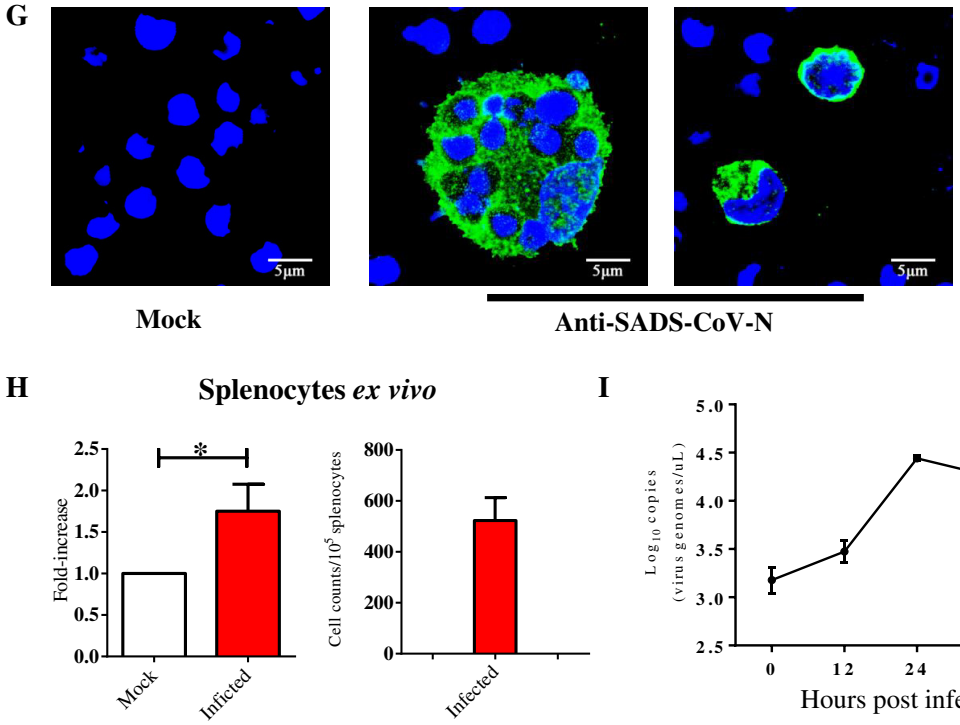

Figure 5

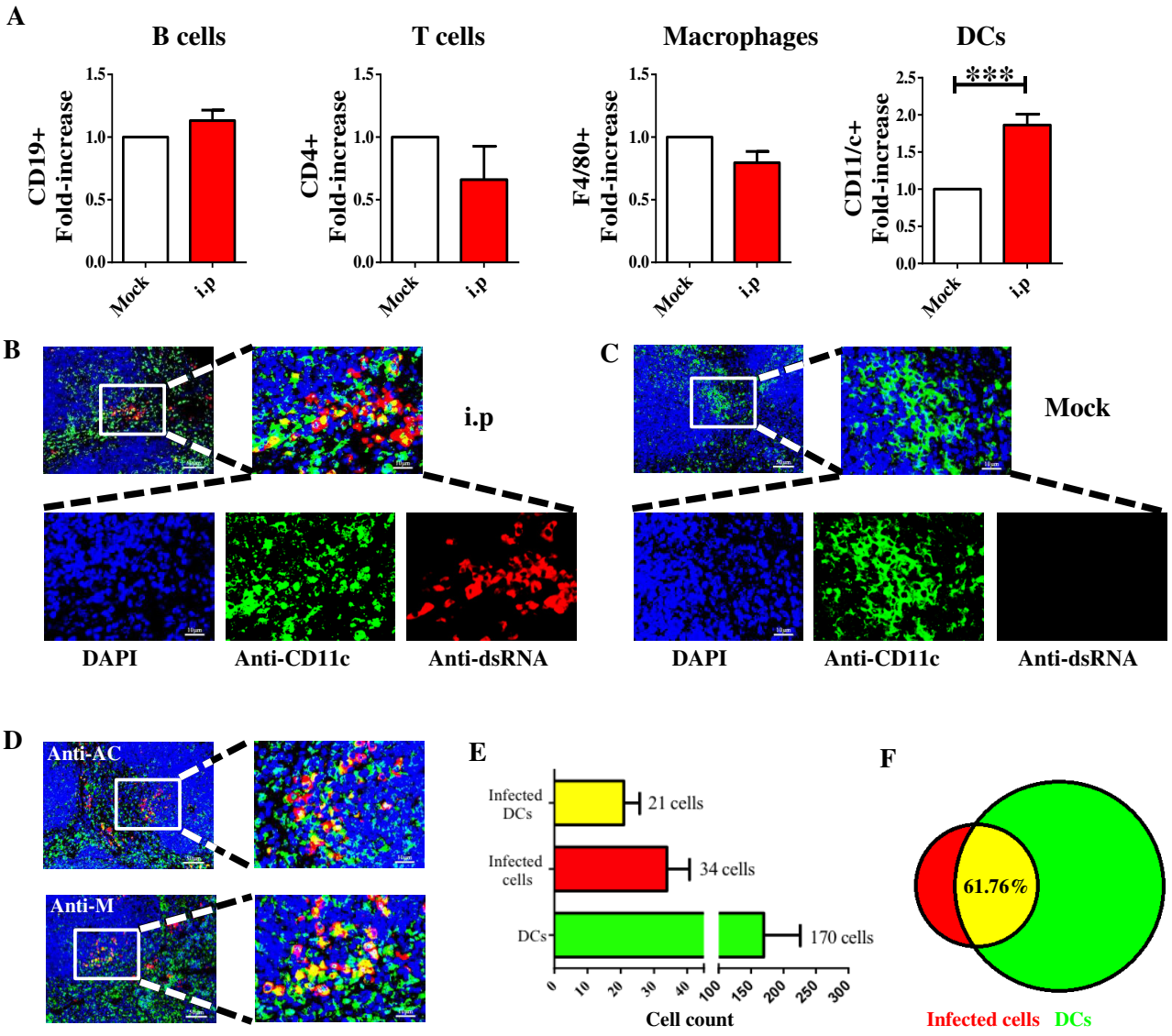

Figure 6